Supporting information for

Amine-based anion receptor enables an improved magnesium plating/stripping reversibility

Tianyi Zhang, Ning Yuan, Zhenfang Zhou, Zhonghua Zhang*, Guicun Li*

[a]*College of Materials Science and Engineering, Qingdao University of Science and Technology, Qingdao 266042, P. R. China.*
*Corresponding authors: zhangzh@qust.edu.cn; guicunli@qust.edu.cn

This file includes the experimental section and Figure S1-S14.

1. Experimental Section

1.1 Electrolyte preparation

To prepare the 0.1 M $Mg(TFSI)_2$/DME electrolyte, 0.1169 g of $Mg(TFSI)_2$ has been dissolved into 2.0 mL DME solvent with consistent magnetic stirring until a clean solution is obtained.

To prepare the 0.1 M $Mg(TFSI)_2$/(DME+FFA) electrolyte, 0.1169 g Mg $(TFSI)_2$ has been dissolved into 2.0 mL of DME and FFA mixed solvents. The volume ratio of DME to furylamine is adjusted to 1:4, 1:1 and 4:1. The $Mg(TFSI)_2$/(DME+FFA) electrolyte in main text represents the 0.1 M $Mg(TFSI)_2$/(DME+FFA) electrolyte with a 1:1 volume ratio of DME to FFA unless otherwise stated. All electrolytes are prepared in a glove box filled with argon gas (water and oxygen content below 0.1 ppm).

1.2 Electrolyte solution and electrodeposits characterizations

Fourier transform infrared (FTIR) tests of electrolyte solution were conducted on a Thermo Scientific Nicolet Apex FT-IR spectrometer. XRD tests were used to determine the phase structure in electrodeposits on a Rigaku D/MAX-2200/PC diffractometer. Morphology of electrodeposits was investigated via Field emission SEM (SEM, JMS6700F). EDS-mapping tests were also conducted on the same equipment. Before characterizations, the electrodeposits were cleaned with THF to remove the residual electrolytes. Surface elemental states of electrodeposits were studied by XPS (XPS, Thermo Fisher Scientific, ESCALAB XI+).

1.3 Electrochemical properties

Typical 2032-type coin-cells were assembled in Ar-filled glove box to test the electrochemical properties. Both copper foil electrode (Cu) and stainless steel (SS) were served as positive electrode to evaluate the Mg plating/stripping properties. Mg foil (0.05 mm in thickness) was served as negative electrode and glass fiber (GF, Whatman) was used as separator. As for the cyclic voltammetry (CV), linear sweep voltammetry (LSV) and electrochemical impedance spectroscopy (EIS) tests, an Autolab PGSTAT302N electrochemcial workstation was used. A scan rate of 5 mV s^{-1} and a voltage range of -1.0 V to 2.0 V were used for CV tests using the Mg//Cu cells. A scan rate of 1.0 mV s^{-1} was used for LSV tests using the Mg//SS cells. An amplitude voltage of 10 mV and frequency range between 0.1 MHz and 10 mHz were used for EIS tests. Chronoamperogram of Mg//SS cells using the $Mg(TFSI)_2$/(DME+FFA) was conducted on the same electrochemical workstation to investigate the diffusion behaviour of Mg^{2+} during Mg nucleation and growth. An overpotential was set at -1.0 V and the current signal was recorded.

1.4 Theoretical calculations

Molecular optimization was performed using the Forcite module in Materials Studio based on density functional theory (DFT). The PBE exchange-correlation functional combined with Grimme's D3 dispersion correction was employed to account for van der Waals interactions, with a plane-wave basis set and a cutoff energy of 500 eV. The optimization targets included 3-furfurylamine (FFA), dimethoxyethane (DME) molecules, as well as complex structures formed by interactions between Mg^{2+} and FFA (monodentate coordination, bidentate coordination), Mg^{2+} and DME, $TFSI^-$ and FFA, $TFSI^-$ and DME, and DME and FFA; stable configurations of each molecule and complex structure were obtained through geometric optimization.

Binding energy calculations were conducted based on the optimized molecules and complex structures, using the same Forcite module and DFT framework with consistent calculation parameters. Specific calculations included binding energies of Mg^{2+} with monodentate-coordinated

FFA, Mg^{2+} with bidentate-coordinated FFA, Mg^{2+} with DME, $TFSI^-$ with FFA, $TFSI^-$ with DME, and DME with FFA. Binding energies were calculated as the difference between the total energy of the complex structure and the energies of its components in their isolated states.

Molecular dynamics (MD) simulations were performed using the Forcite module in Materials Studio with the COMPASS force field. Coarse-grained models of 0.1 M $Mg(TFSI)_2$/DME electrolyte and 0.1 M $Mg(TFSI)_2$/(DME+FFA) electrolyte were constructed, and simulations were conducted under the NPT ensemble for 100 ns with a time step of 1 fs. Amorphous cell module has been used to build a solution box, which contains 3 Mg^{2+} molecules, 6 $TFSI^-$ molecules, 194 DME molecules for the $Mg(TFSI)_2$/DME electrolyte. As for $Mg(TFSI)_2$/(DME+FFA) electrolyte, the same module has been used to build the solution box, which contains 3 Mg^{2+} molecules, 6 $TFSI^-$ molecules, 103 DME molecules, 91 FFA molecules. Radial distribution functions (RDFs) were obtained by analyzing MD simulation trajectories, focusing on RDFs of Mg^{2+} with O atoms in DME (Mg-O), Mg^{2+} with O atoms in $TFSI^-$ (Mg-O), and Mg^{2+} with N atoms in FFA (Mg-N) to characterize the solvation environment of Mg^{2+}, while snapshots from MD simulations were used to visually display solvation sheath structures. The coordination numbers of various ligands to Mg^{2+} are calculated within a range of 3.0 Å between Mg^{2+} and ligand in radial distribution function plots.

Electrostatic potential (ESP) calculations were performed using the DMol3 module in Materials Studio based on DFT theory, adopting the same PBE functional and D3 dispersion correction as the above calculations. The calculation targets were FFA and DME molecules; charge distribution analysis was conducted on the optimized molecular structures to obtain ESP values on the molecular surface, with a focus on maximum negative ESP values at the N atom center in FFA and the O atom center in DME to analyze the charge distribution characteristics of the molecules.

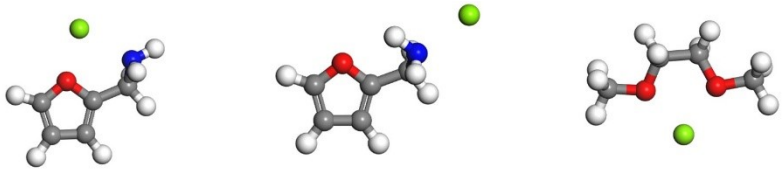

Figure S1 The structural configurations and the corresponding binding energies between Mg^{2+} and solvents.

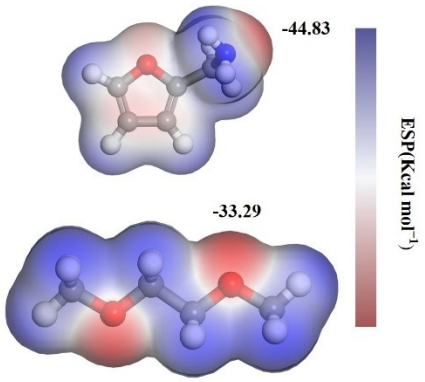

Figure S2 The electrostatic potential (ESP) values of FFA and DME solvents.

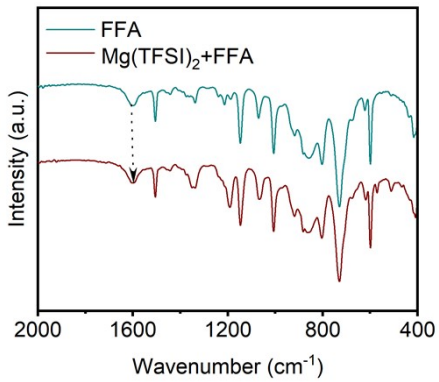

Figure S3 Fourier transform infrared (FTIR) spectra of FFA and $Mg(TFSI)_2$/FFA electrolyte.

Fourier transform infrared (FTIR) spectra in Fig. S3 reveal a clear blue shift for the N-H in-plane bend signal in FFA molecule after introducing $Mg(TFSI)_2$ into FFA solvent, indicating a possible hydrogen bonding interaction between them.

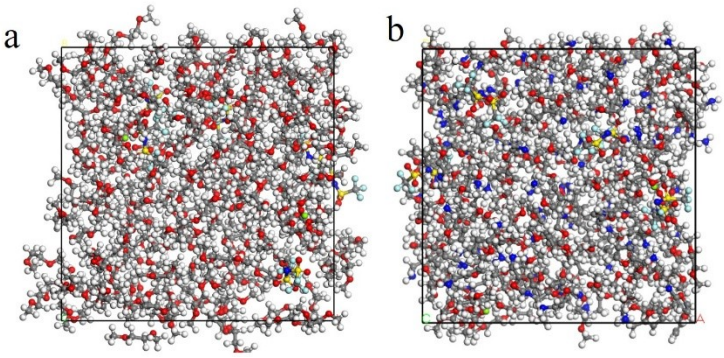

Figure S4 The snapshots of MD simulation results for both $Mg(TFSI)_2$/DME electrolyte (a) and $Mg(TFSI)_2$/(DME+FFA) electrolyte (b).

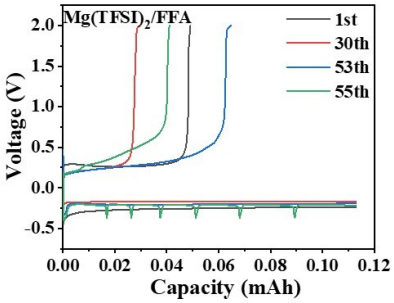

Figure S5 The charge and discharge profiles of Mg//Cu cells with $Mg(TFSI)_2$/FFA electrolyte.

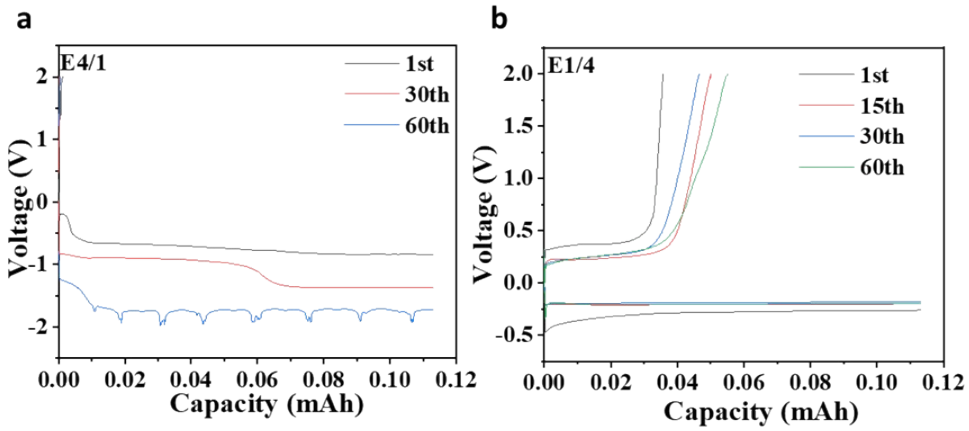

Figure S6 (a) The charge/discharge profiles of 1st, 30th and 60th cycles at 1.0 mA cm^{-2} for $Mg(TFSI)_2$/(DME+FFA) electrolyte with DME:FFA volume ratio of 4:1. (b) The charge/discharge profiles of 1st, 15th, 30th and 60th cycles at 1.0 mA cm^{-2} for $Mg(TFSI)_2$/(DME+FFA) electrolyte with DME:FFA volume ratio of 1:4.

With different volume ratios of FFA and DME solvents (4:1 and 1:4), the Mg//Cu cells (Fig. S6) also show better Mg plating/stripping properties, but they are inferior to electrolytes with DME and FFA volume ratio of 1:1.

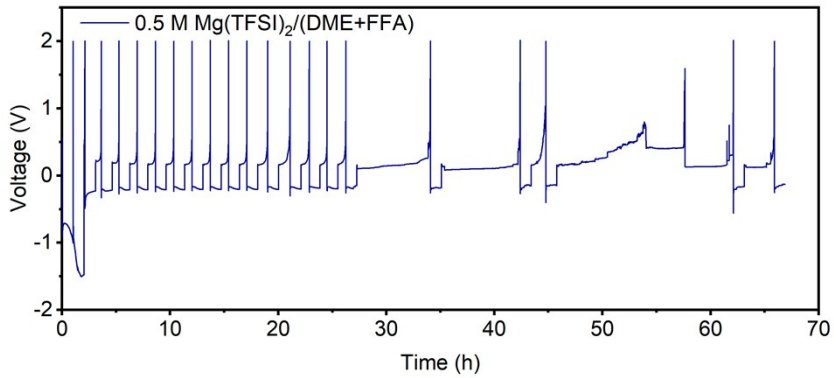

Figure S7 Voltage-time profile of Mg//Cu cells using 0.5 M $Mg(TFSI)_2$/(DME+FFA) electrolyte.

Under a higher concentration of 0.5 M, the Mg//Cu cells using $Mg(TFSI)_2$/(DME+FFA) electrolyte show a limited cycle lifespan of only 14 cycles (Figure S7), which might relate to the formation of more Mg^{2+}-$TFSI^-$ ion pairs compared to the low concentration electrolytes.

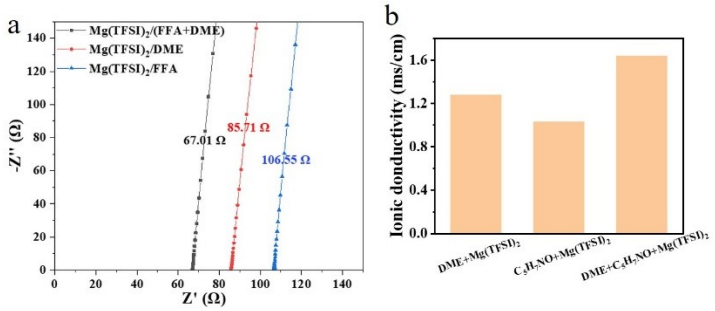

Figure S8 (a) EIS results of symmetric SS//SS cells with different electrolytes. (b) Ionic conductivities of varied electrolytes.

Ionic conductivity is calculated according to formula (σ=l/(S*R)), in which σ, l, S and R represent ionic conductivity (mS cm^{-1}), thickness of separator (0.22 cm), area of separator (2.01 cm^2) and resistance of the cell as examined in Figure S8a. The $Mg(TFSI)_2$/(DME+FFA) electrolytes show a highest ion conductivity of 1.63 mS cm^{-1} (1.01 mS cm^{-1} for $Mg(TFSI)_2$/FFA and 1.28 mS cm^{-1} for $Mg(TFSI)_2$/DME) as shown in Figure S8b.

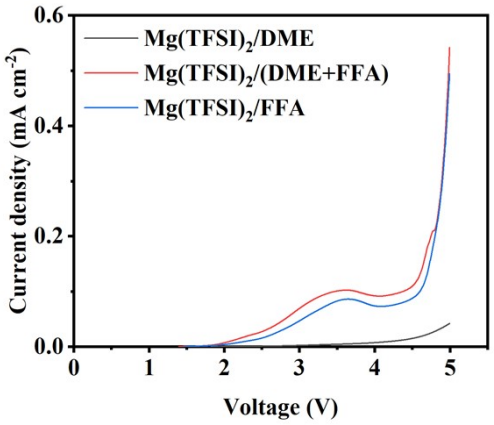

Figure S9 LSV curves of Mg//SS cells with varied electrolytes.

Linear scanning voltammetry (LSV) results in Figure S9 reveal that Mg//SS cells show an inferior electrochemical potential window (2.4 V for $Mg(TFSI)_2$/(DME+FFA) and 2.5 V for $Mg(TFSI)_2$/FFA compared to the $Mg(TFSI)_2$/DME electrolyte (4.0 V), which might be due to the potential hydrogen evolution reaction of amine-based electrolytes.

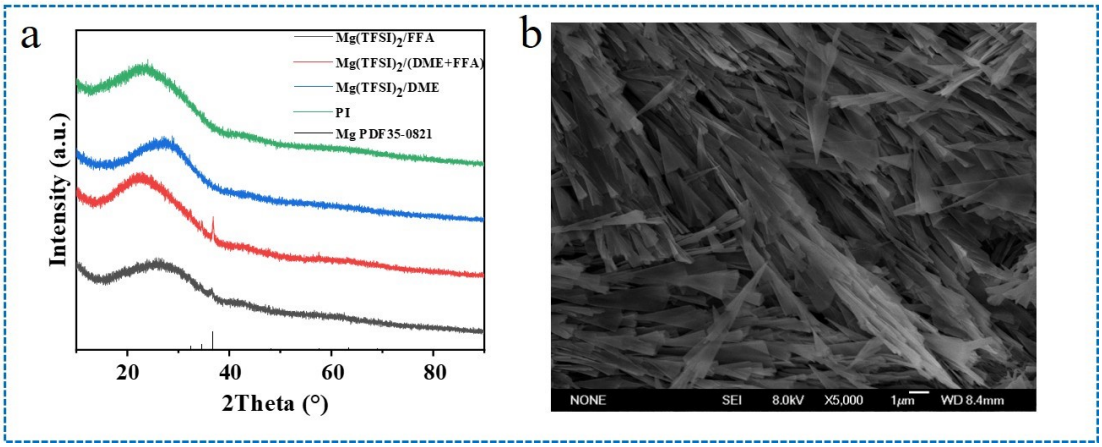

Figure S10 XRD patterns (a) and SEM images (b) of electrodeposits from varied electrolyte.

X-ray diffraction (XRD) patterns of electrodeposits from both $Mg(TFSI)_2$/FFA and $Mg(TFSI)_2$/(DME+FFA) in Figure S10a show highly crystalline Mg metal phases (PDF#35-0821), indicating the Mg^{2+} electro-plating. In contrast, XRD pattern of deposition products from $Mg(TFSI)_2$/DME electrolyte show no crystal diffraction peaks, suggesting the passivation of Mg-metal anodes. These results are consistent with the above electrochemical results.

Post-scanning electron microscopy (SEM) analyses (Figure S10b) reveal that there are irregular dendritic products on Cu current collector. The corresponding EDS mapping images in Figure S11 show that the main components of the dendritic products are Mg and O with trace F species, which are consistent with above XPS results. It is supposed that the dendrite growth of Mg during plating process leads to the final short circuit.

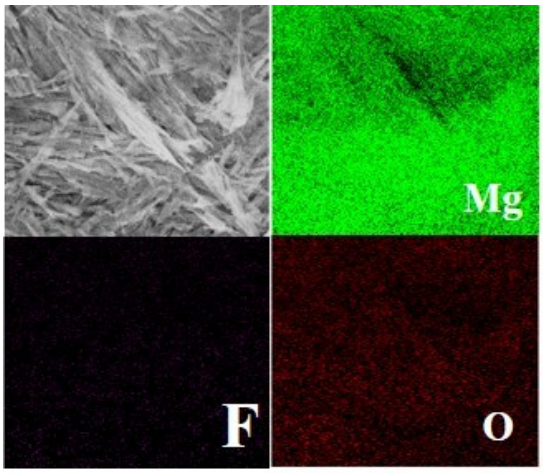

Figure S11 Typical SEM images and the corresponding EDS-mapping images.

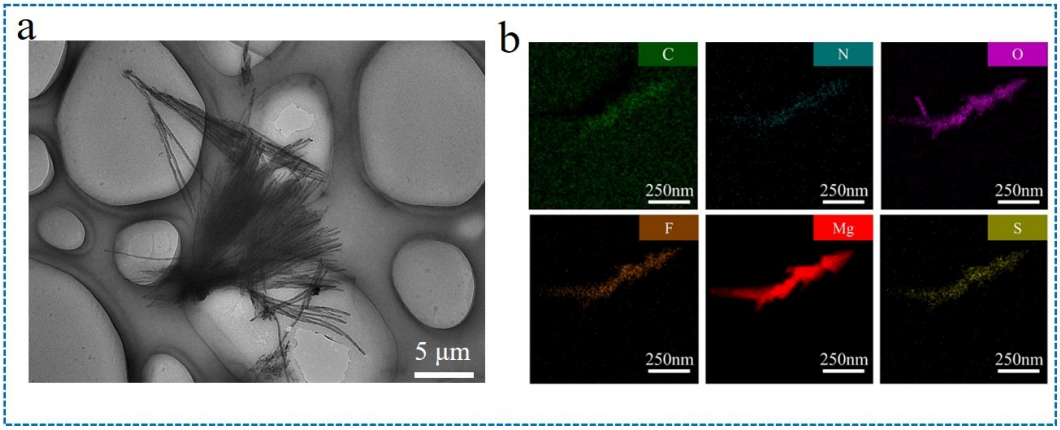

Figure S12 TEM (a) and EDS-mapping images (b) of electrodeposits from varied electrolyte.

Transmission electron microscopy (TEM) image of electrodeposits from $Mg(TFSI)_2$/(DME+FFA) also reveal the needle-like morphology (Figure S12a), which is consistent with the dendritic phase in SEM image (Figure S0b). The corresponding EDS-mapping images (Figure S12b) and the profile (Figure S13) demonstrate the existence of elements including C, N, O, F and S, indicating the concomitant decomposition of electrolyte during Mg plating process.

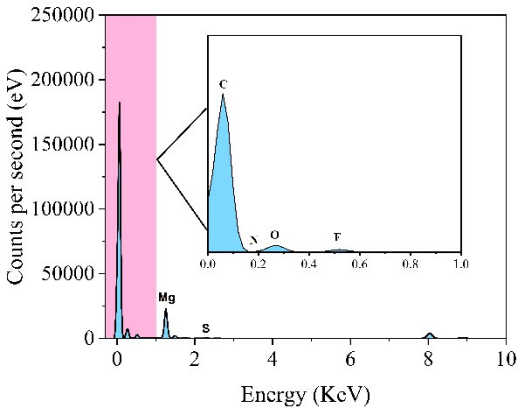

Figure S13 The EDS profile of the electrodeposits from $Mg(TFSI)_2$/(DME+FFA) electrolyte.

Discussion on the relationships between the Mg plating/stripping performances and electrolyte solution species is listed below.

The better Mg plating/stripping performance for $Mg(TFSI)_2$/(DME+FFA) electrolyte is predominantly ascribed to the improved interphase chemistry. It is assumed that the competitive decomposition of both $TFSI^-$ and DME solvent contributes to the interfacial passivation facing Mg-metal anode. It is expected that organic-rich interphases might be generated from the decomposition of DME and inorganic-based interphases might be formed due to the decomposition of $TFSI^-$, which have been proved by the XPS analyses in Fig. 3 and Figure S11-S12. In consideration of the flexibility, ion penetrability and solubility, the organic interphases show better compatibility towards Mg-metal anode compare to the inorganic counterparts. By associating with $TFSI^-$, the FFA plays a key role in regulating the formation of anion-less Mg^{2+} solvation structure, which greatly

suppress the interfacial passivation by inorganic interphases from the decomposition of $TFSI^-$. Therefore, a balanced interfacial stability and Mg plating/stripping performance has been achieved for the $Mg(TFSI)_2$/(DME+FFA) electrolyte, although some improvements are needed further to meet the criteria of practical application.

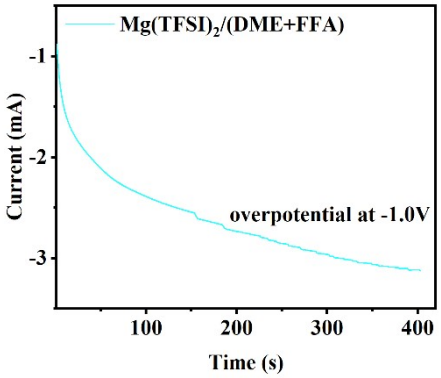

Figure S14 Chronoamperogram of Mg//SS cells using the $Mg(TFSI)_2$/(DME+FFA).

As shown in Figure S14, chronoamperogram of Mg//SS cells using the $Mg(TFSI)_2$/(DME+FFA) reveal the continuously decreased current response for more than 400 s, suggesting an incessant 2D diffusion on the electrode surface. Due to the competitive decomposition of electrolyte species and Mg plating reactions, the unstable interfacial film might be repeatedly destructed, which helps to expose highly active tips for dendrite growth.